Torque-Ripple Minimization for Permanent-Magnet Synchronous Motors Based on Harmonic Flux Estimation

Mojgan Nikouie, Oskar Wallmark, Lennart Harnefors
Department of Electric Power and Energy Systems
KTH Royal Institute of Technology, Stockholm, Sweden
{mojgann, owa, lhar}@kth.se

Keywords Flux estimation, PIR current controller, Torque ripple

Abstract This paper presents a control algorithm to reduce the torque ripple in permanent-magnet synchronous motors. This control algorithm is based on the on-line estimation of harmonic flux linkage. Together with the on-line estimation of the flux linkage, a proportional–integral–resonant controller is introduced to suppress the torque ripple.

1 Introduction

The design and development of different topologies for integrated modular electric drives (IMED) has increased rapidly during the last decade. IMEDs are very attractive solutions for different industrial and traction applications [1–3]. Integration between the converter and the electric machine gives the benefit of a compact system with lower size and weight, as well as lower electro-magnetic interference (EMI) due to removal of the cables.

In [4], a new IMED topology for electric vehicles (EVs) and hybrid electric vehicles (HEVs) is proposed. This topology is an integration between a stacked polyphase bridges (SPB) converter and a fractional-slots concentrated-windings (FSCW) permanent-magnet synchronous motor (PMSM), see Figure 1.

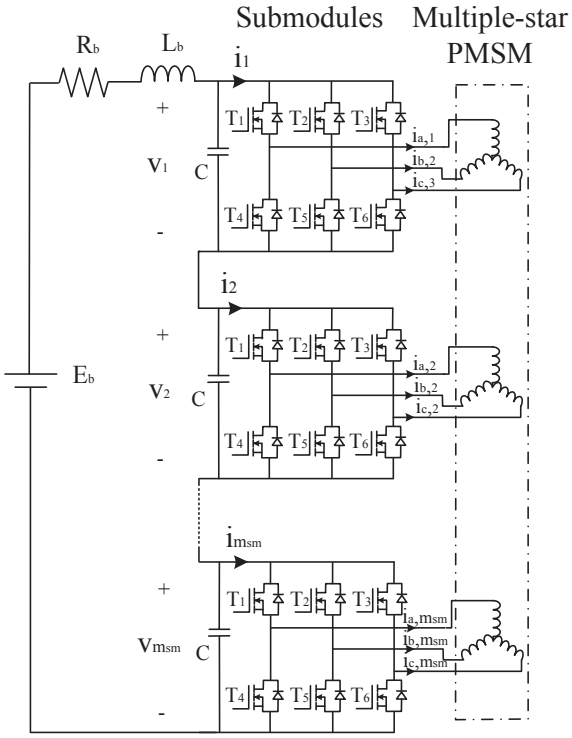

Figure 1: Schematic diagram of the proposed IMED topology (integration between SPB converter and FSCW PMSM).

The SPB converter consists of a certain number, m_{sm}, of submodules that are connected in series on the dc side. Each submodule consists of a two-level, three-phase converter that is connected to a set of three-phase windings in the motor. This converter structure allows the usage of low-voltage components, such as metal-oxide

semiconductor field-effect transistors (MOSFETs) utilizing a high switching frequency (up to around 100 kHz). This gives the opportunity to use a very small, low-voltage film, or perhaps ceramic, capacitor for each submodule.

In [5], the design for the FSCW PMSM is presented. The study identifies the suitable phase/slot/pole combination to be used along with SPB converter, and also the potential benefits are reported. However, it is mentioned that disadvantages of the FSCW PMSM include relatively high iron losses and the presence of torque ripple.

Generally, in PMSMs, relative large torque ripple can be produced by spatial harmonics of the air-gap reluctance and of the magnetic flux linkage, as well as by harmonics in the stator current [6]. Torque ripple causes noise and mechanical vibrations which can reduce the life span of the motor and affect other mechanical components affixed to the motor shaft [7].

It is possible to reduce the torque ripple in PMSMs, but it is impossible to entirely eliminate it. Research studies on both machine design and control algorithms have resulted in proposals for several methods to reduce the torque ripple. Using a skewed rotor, distributed windings, and careful design of slot poles are suggested for motor design. However, considering all these aspects in the design may cause a high production cost and special manufacturing techniques [8].

Control methods, on the other hand, offer a cheaper solution for torque-ripple minimization. In [9], a method to reduce torque ripple using harmonic injected current instead of sinusoidal current is proposed. It is shown that the torque ripple is reduced. However, using this method, obtaining the amplitude of the dominant-order current harmonic is needed. In addition, several iterative numerical analyses are needed in order to reduce the torque ripple. A mathematical method for torque-ripple minimization is proposed in [10]. In this method, optimal currents are derived from the torque or speed control strategies based on Adaline neural networks. To deduce the torque ripple according to [10] is very complicated and it seems not to be a user-friendly method.

An interesting method for torque-ripple reduction is presented in [11]. The q-axis (i.e., the torque-producing) current component reference is defined based on the torque reference divided by q-axis back-electromotive force (EMF). This back EMF includes harmonics and is measured off-line and stored in the memory of the digital control system. The division in calculating the q-axis current component helps to remove the ripple in the torque by injecting harmonics in the current. Therefore, the authors introduce a repetitive current controller in order to correctly track the current reference. The repetitive current controller is an effective method for tracking the periodic reference and compensating periodic disturbances. The repetitive current controller is merged to the proportional–integral (PI) controller, where the PI control dominates during transients and large signal dynamics, while the repetitive control ensures the compensation of the remaining errors so as to achieve a near perfect tracking of a the periodic current reference signal. While the method suggested in [11] is straightforward and effective, the main drawback is the need to measure the back-EMF off-line, as mentioned before.

This paper presents an extension to the technique that is introduced in [11]. The idea is, instead of measuring the back-EMF off-line, it can be estimated on-line. There is no need for commissioning, except that a good estimate of the q-axis inductance is needed. Although this paper presents results for a specific motor—the FSCW PMSM—the method is general for all PMSM types. The paper is organized as follows. Section 2 presents the PMSM model and the mathematical details to generate the current reference for torque-ripple minimization. Section 3 shows the simulations. Experimental results are presented in Section 4. Section 5 contains a conclusion.

2 Control System Design

2.1 PMSM Model

The PMSM model in the dq reference frame is given as

$$v_{sd} = R_s i_{sd} + \frac{d\psi_d}{dt} - \omega_e \psi_q \qquad v_{sq} = R_s i_{sq} + \frac{d\psi_q}{dt} + \omega_e \psi_d \tag{1}$$

where i_{sd} and i_{sq} are the dq-axes stator current components, v_{sd} and v_{sq} are the dq-axes voltage components, R_s is the stator resistance, ω_e is the electrical angular velocity (which is related to the mechanical angular velocity, ω_m, as $\omega_e = p\omega_m$, where p is the number of pole pairs), and ψ_d and ψ_q are the flux linkage components, respectively. These components can be expressed as

$$\psi_d = L_d i_{sd} + \psi_m + \psi_{mdh} \qquad \psi_q = L_q i_{sq} + \psi_{mqh} \tag{2}$$

where ψ_m is the fundamental component and ψ_{mdh} and ψ_{mqh} are the harmonic components. L_d and L_d are the dq-axes inductances. The electrical torque is given as

$$T_e = \frac{3p}{2}\left(\psi_d i_{sq} - \psi_q i_{sd}\right). \tag{3}$$

The component i_{sd} is controlled to zero, since it is assumed that $L_d - L_q$ is relatively small and therefore the reluctance-torque contribution is minor.

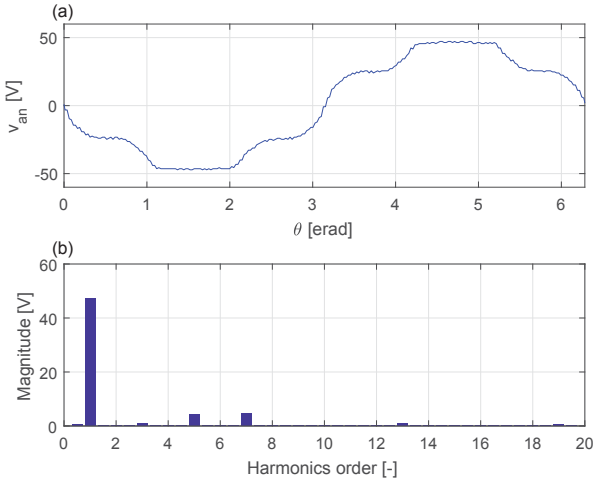

Figure 2: Harmonic analysis in stator winding of FSCW PMSM; (a) phase voltage, (b) harmonic order.

As mentioned before, the harmonics that are present in the air-gap flux have the largest share in producing torque pulsations compared to the cogging torque. The trapezoidal flux linkage has harmonics of the orders $5,7,11,\ldots$ (Harmonic orders of multiple three are absent in the Y-connected stator windings.) In the dq reference frame, harmonic orders of multiple six appear, and can be expressed as

$$\begin{aligned}\psi_{mdh} &= \psi_{md6}\cos(6\theta_e+\varphi_{d6})+\psi_{md12}\cos(12\theta_e+\varphi_{d12})+\cdots\\ \psi_{mqh} &= \psi_{mq6}\sin(6\theta_e+\varphi_{q6})+\psi_{mq12}\sin(12\theta_e+\varphi_{q12})+\cdots\end{aligned} \tag{4}$$

where $\psi_{md,q6}$ and $\psi_{md,q12}$ are the sixth- and twelfth-order harmonics magnitudes respectively of the dq-axis flux-linkage component, θ_e is the electrical angle, and $\varphi_{d,q6}$ and $\varphi_{d,q12}$ are phase shifts. Normally, the sixth-order harmonic is dominant. This is exemplified in Figure 2 for the FSCW PMSM prototype under consideration. Therefore, only the sixth-order harmonic is considered in the following.

Although the component ψ_q consists of harmonic orders of multiples of six, it does not influence the torque ripple. The reason is that the current component i_{sd} is controlled to zero, see (3).

2.2 Estimator Design

Remember that in the method that is proposed in [11], the d-direction flux is calculated off-line and the back EMF, $e_d = \omega_e\psi_d$ is stored in a memory. However, it is possible to estimate ψ_d on-line. From the first relation of (1), we have

$$\psi_d = \int (v_{sd} - R_s i_{sd} + \omega_e\psi_q)\, dt. \tag{5}$$

This equation forms the basis for the estimation. As the first step, v_{sd} is replaced by the reference voltage component (from the current controller) v_{sd}^{ref}, because the stator voltage is normally not measured, $i_{sd}=0$ is applied, and L_q is replaced by its estimated value $\hat{L}_q$. Concerning the q-direction flux linkage, the harmonic term ψ_{mqh} is unknown. However, in the first relation of (1), the harmonic term of $d\psi_d/dt$ will dominate over the harmonic term in $\omega_e\psi_q$, because differentiation gives an amplification of the amplitude by the harmonic order, i.e., a multiple of 6. Therefore, we may approximate $\psi_q \approx L_q i_{sq}$ in (5), giving the estimated value of ψ_d as

$$\hat{\psi}_d = \int \left(v_{sd}^{\text{ref}} + \hat{L}_q i_{sq}\right) dt. \tag{6}$$

Equation (6) involves a pure integration, which is marginally stable. If the 6th harmonic only is considered, this can be avoided by adding a band-pass filter to (6)

$$H_{\text{BP}}(s) = \frac{\omega_b s}{s^2+\omega_b s+(6\omega_e)^2} \tag{7}$$

where $s = d/dt$ (or the Laplace variable, where appropriate) and ω_b is the filter bandwidth. Notice that $H_{\text{BP}}(j6\omega_e) = 1$, meaning that the output signal for the specific frequency $6\omega_e$ will be equal to the input signal in the steady state. Introducing the band-pass filter in (6) and adding the estimate $\hat{\psi}_m$ of ψ_m (which is constant) yields

$$\hat{\psi}_d = \frac{\omega_b}{s^2+\omega_b s+(6\omega_e)^2}\left(v_{sd}^{\text{ref}} + \hat{L}_q i_{sq}\right) + \hat{\psi}_m. \tag{8}$$

We see that integration and band-pass filtering gives a low-pass filter, meaning that the estimation will be asymptotically stable.

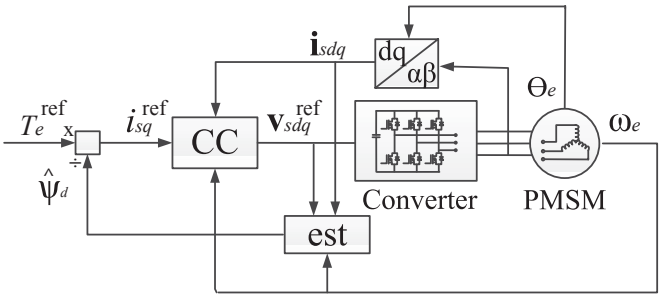

Figure 3: Schematic diagram of the current control (CC) and estimation (est) system.

2.3 Torque-Producing Current Reference Selection

From (3), the reference for the torque-producing stator current component i_{sq}^{ref} is obtained as a function of the torque reference T_e^{ref} and the estimated flux linkage as

$$i_{sq}^{\text{ref}} = \frac{2}{3p\hat{\psi}_d} T_e^{\text{ref}}. \tag{9}$$

2.4 Current Controller Design

The state of the art for current control is to select a proportional–integral (PI) controller. However, in this case using a PI controller is not sufficient. A PI controller fails to track a sinusoidal reference accurately [12]. Remember that i_{sq}^{ref} contains a $6\omega_e$ component, see (9). Therefore, we select a proportional–integral–resonant (PIR) controller. This means that a resonant term with angular resonant frequency $6\omega_e$ is added in parallel to the PI terms to improve current controller performance. The algorithm for the current controller is given as

$$\begin{aligned} v_{sd}^{\text{ref}} &= \left(K_{pd} + \frac{K_{id}}{s} + \frac{K_{rd}s}{s^2+(6\omega_e)^2}\right)\left(i_{sd}^{\text{ref}} - i_{sd}\right) - R_{ad}i_{sd} - \omega_e\hat{L}_q i_{sq} \\ v_{sq}^{\text{ref}} &= \left(K_{pq} + \frac{K_{iq}}{s} + \frac{K_{rq}s}{s^2+(6\omega_e)^2}\right)\left(i_{sq}^{\text{ref}} - i_{sq}\right) - R_{aq}i_{sq} + \omega_e\hat{L}_d i_{sd} \end{aligned} \tag{10}$$

where $K_{pd} = \alpha_c\hat{L}_d$ and $K_{pq} = \alpha_c\hat{L}_q$ are the proportional gains, $K_{id} = \alpha_c^2\hat{L}_d$ and $K_{iq} = \alpha_c^2\hat{L}_q$ are the integral gains, $K_{rd} = \alpha_r K_{pd}$ and $K_{rq} = \alpha_r K_{pq}$ are the resonant gains, and $R_{ad} = K_{pd}$, $R_{ad} = K_{pq}$ are the active resistances in the dq axes, respectively. Finally, α_c and α_r are the bandwidths of the current control loop and the resonator, respectively.

3 Simulation Results

To verify the proposed algorithm, a simulation model for one submodule of the SPB converter and one set of three-phase windings of the FSCW PMSM has been implemented in Matlab/Simulink. The parameters that are used in the simulation are listed in Table 1.

Table 1: Parameters

p	4		number of pole pairs
L_d	0.4	mH	d-direction inductance per submodule
L_q	1.4	mH	q-direction inductance per submodule
R_s	18.6	mΩ	stator resistance per submodule
n_m^{nom}	4000	rpm	rated mechanical velocity
ω_e^{nom}	1676	rad/s	rated electrical angular velocity
ψ_m	0.0203	Vs	flux linkage per submodule
f_{sw}	20	kHz	switching frequency
α_c	219.72	rad/s	bandwidth of current control loop
α_r	21.9	rad/s	bandwidth of resonator
ω_b	20	rad/s	bandwidth of filters
T_e	-25	Nm	torque reference per submodule

In order to see the influence of the proposed algorithm on the suppression of the torque ripple, three different simulations, respectively with PI controller, PIR controller, and finally PIR controller together with the on-line flux

estimator, are studied. Results for this study are shown in Figure 4. As can be seen in Figure 4-a) ripples on i_{dq} and T_e are quite significant when the PI controller is used. Figures. 4-b) and c) are verifying the fact that using the PIR controller is the better controller choice for reducing ripples on both current references and torque, even without the proposed flux estimator. Activating the on-line flux estimator increases the current ripples slightly, but torque ripples are suppressed more.

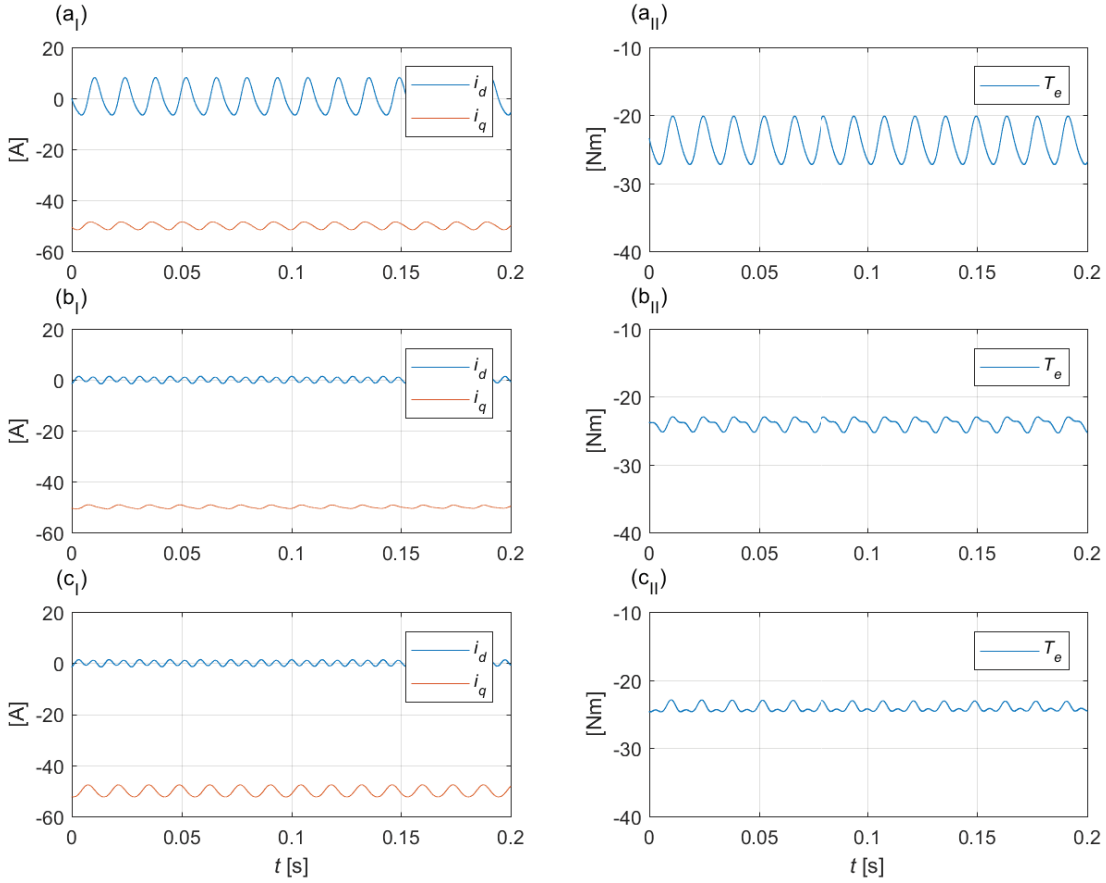

Figure 4: Simulation results for (a) PI control, (b) PIR control, and (c) PIR control with harmonic flux estimation.

4 Experimental Results

Figure 5 shows the experimental setup for the integrated drive under consideration. As shown, the SPB converter with four submodules is connected to the end windings of the FSCW PMSM. The converter's water cooling and an enclosure for the current sensors are installed between the motor end windings and the converter. Therefore, the design benefits of reducing EMI effects. Reference [13] explains the design in detail.

However, for this study one submodule was connected to the motor as shown in Figure 6-b). Similar to the simulation part, three different control algorithms, PI controller, PIR controller, PIR controller together with on-line flux estimator, are programmed on the microprocessor which is located on the SPB control board. Then, phase current and torque are measured by the current and torque sensors respectively. Speed of the motor for this experiment was controlled by a servomotor which is connected as a load to the FSCW PMSM. This means that there is no speed controller is designed for the prototype. The speed reference was set to 3 Hz mechanical frequency.

The experimental results are shown in Figure 7. As can be seen, the phase current is completely sinusoidal when the PIR controller is selected and it has a slightly deformed waveform when using the other two controller. (The deformation for PIR controller with the on-line estimator is caused by the latter by purpose.) Unlike in the simulations, the torque ripples at the sixth harmonic are quite difficult to determine from the figures, because of strong ripple components at higher frequency. Therefore, the torque signals are analyzed using the discrete Fourier transform (DFT). The results from the DFT are illustrated in Figure 8. It is clearly shown that the DFT for the control algorithm where the PIR controller plus the on-line flux estimator is used has the lowest value at the sixth harmonic, which corresponds to 3 Hz mechanical frequency $\times$ 4 pole pairs $\times$ harmonic order 6, i.e., 72 Hz.

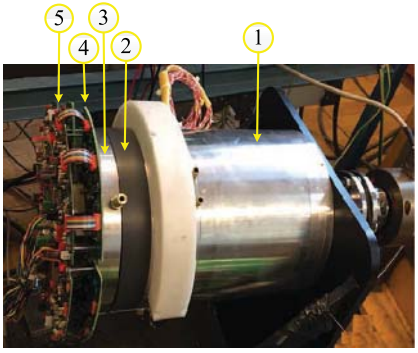

Figure 5: The proposed IMED topology; 1: electric motor (FSCW PMSM), 2: current sensors enclosure, 3: water cooling plates, 4: power boards, 5: control boards.

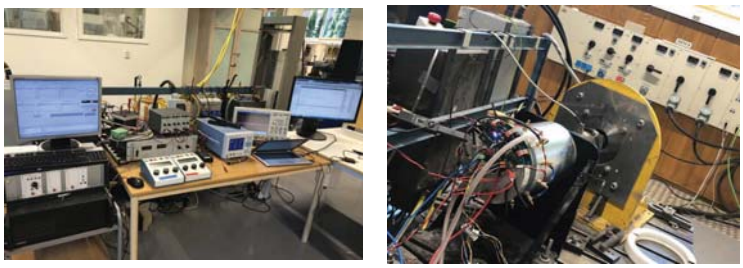

a) b)

Figure 6: Experimental setup (a) power supplies and control set up, (b) FSCW PMSM connected to one submodule.

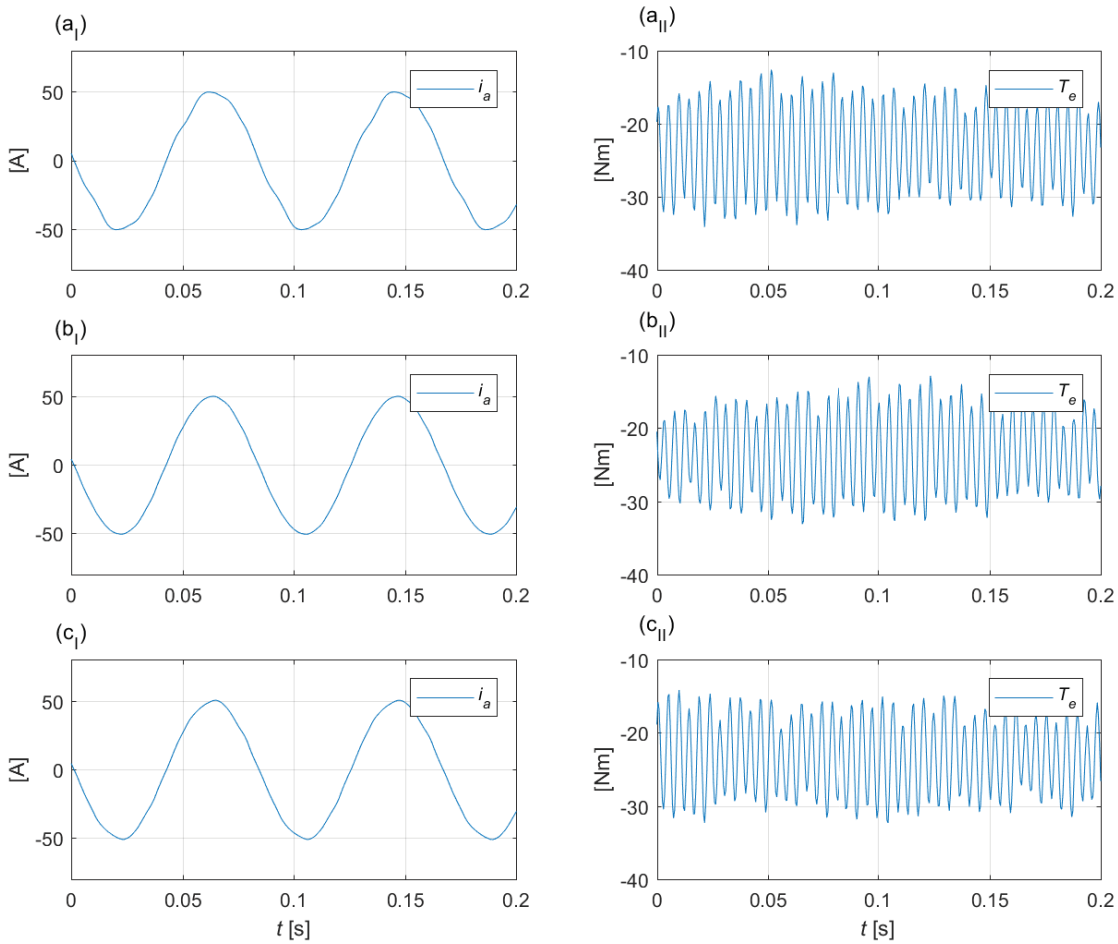

Figure 7: Experimental results for (a) PI control, (b) PIR control, and (c) PIR control with harmonic flux estimation.

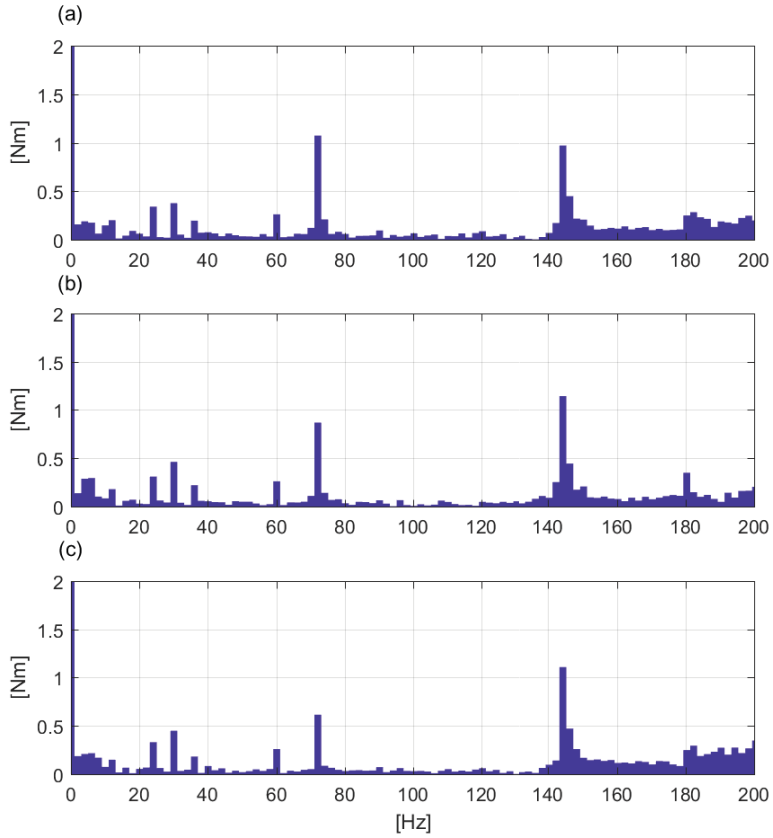

Figure 8: Spectra of the measured torque with (a) PI control, (b) PIR control, and (c) PIR control with harmonic flux estimation.

5 Conclusion

This paper presents an algorithm for a controller to reduce the torque ripple in a PMSM. The proposed algorithm is an extension of the technique that is introduced in [11]. In PMSMs the harmonics in the stator current and as well as the space harmonics of the air-gap reluctance and the flux linkage produce the torque ripple. The reference for the q-axis current component, which is torque producing, is set based on the reference torque divided by the back EMF. The back EMF is proportional to the flux linkage and its harmonics. In [11], the back-EMF is estimated off-line and stored in a memory. This paper instead proposes an on-line estimation of the flux linkage and its harmonics. In this method, unlike in [11], there is no need for commissioning, except an accurate estimate of the q-axis inductance. The algorithm should be used with a PIR current controller.

References

[1] S. Gjerde and T. Undeland, "Power conversion system for transformer-less offshore wind turbine," in *Proceedings of the 14th European Conference on Power Electronics and Applications (EPE 2011)*, Aug. 2011.

[2] Y. Han, "Design, modeling, and control of multilevel converter motor drive with modular design and split winding machine," in *Proceedings of the IEEE 15th Workshop on Control and Modeling for Power Electronics (COMPEL 2014)*, Jun. 2014.

[3] J. A. Rosero, J. A. Ortega, E. Aldabas, and L. Romeral, "Moving towards a more electric aircraft," *IEEE Aerospace and Electronic Systems Magazine*, vol. 22, no. 3, pp. 3–9, Mar. 2007.

[4] S. Norrga, L. Jin, O. Wallmark, A. Mayer, and K. Ilves, "A novel inverter topology for compact EV and HEV drive systems," in *39th Annual Conference of the IEEE Industrial Electronics Society, (IECON 2013)*, Nov. 2013, pp. 6590–6595.

[5] H. Zhang, O. Wallmark, M. Leksell, S. Norrga, M. Nikouie, and L. Jin, "Machine design considerations for an MHF/SPB-converter based electric drive," in *40th Annual Conference of the IEEE Industrial Electronics Society (IECON 2014)*, Oct. 2014, pp. 3849–3854.

[6] A. Mora, A. Orellana, J. Juliet, and R. Cardenas, "Model predictive torque control for torque ripple compensation in variable-speed PMSMs," *IEEE Transactions on Industrial Electronics*, vol. 63, no. 7, pp. 4584–4592, Jul. 2016.

[7] A. Gebregergis, M. H. Chowdhury, M. S. Islam, and T. Sebastian, "Modeling of permanent-magnet synchronous machine including torque ripple effects," *IEEE Transactions on Industry Applications*, vol. 51, no. 1, pp. 232–239, Jan. 2015.

[8] H. Dhulipati, S. Mukundan, K. L. V. Iyer, and N. C. Kar, "Skewing of stator windings for reduction of spatial harmonics in concentrated wound PMSM," in *30th IEEE Canadian Conference on Electrical and Computer Engineering (CCECE, 2017)*, Apr. 2017, pp. 1–4.

[9] G. H. Lee, S. I. Kim, J. P. Hong, and J. H. Bahn, "Torque ripple reduction of interior permanent magnet synchronous motor using harmonic injected current," *IEEE Transactions on Magnetics*, vol. 44, no. 6, pp. 1582–1585, Jun. 2008.

[10] D. Flieller, N. K. Nguyen, P. Wira, G. Sturtzer, D. O. Abdeslam, and J. Merckle, "A self-learning solution for torque ripple reduction for nonsinusoidal permanent-magnet motor drives based on artificial neural networks," *IEEE Transactions on Industrial Electronics*, vol. 61, no. 2, pp. 655–666, Feb. 2014.

[11] P. Mattavelli, L. Tubiana, and M. Zigliotto, "Torque-ripple reduction in PM synchronous motor drives using repetitive current control," *IEEE Transactions on Power Electronics*, vol. 20, no. 6, pp. 1423–1431, Nov. 2005.

[12] T. M. Rowan and R. J. Kerkman, "A new synchronous current regulator and an analysis of current-regulated PWM inverters," *IEEE Transactions on Industry Applications*, vol. IA-22, no. 4, pp. 678–690, Jul. 1986.

[13] M. Nikouie, H. Zhang, O. Wallmark, and H. P. Nee, "Highly integrated electric drives system for tomorrow's EVs and HEVs," in *Proceedings of the 3rd Southern Power Electronics Conference (SPEC 2017)*, Dec. 2017.